High Frequency (HF) Radio Astronomy from a Small Satellite

Frank C. Robey[1], Mary Knapp[2], Alan J. Fenn[1], Mark Silver[1], Kerry Johnson[1],
Frank J. Lind[3], Ryan Volz[3], Sara Seager[2], Farshid Neylon-Azad[1]
Massachusetts Institute of Technology

[1] Lincoln Laboratory
Lexington, MA
781-981-7865
robey@ll.mit.edu

[2]Earth, Atmosphere and
Planetary Science
Cambridge, MA
Knapp@mit.edu

[3]Haystack Observatory
Westford, MA
flind@haystack.mit.edu

ABSTRACT

The low frequency portion of the electromagnetic spectrum (below 15 MHz) is poorly explored due to the opacity of the Earth's ionosphere and the need for large interferometric baselines to achieve useful angular resolution and sensitivity. A wide range of science topics would greatly benefit from measurements in this band, including magnetospheric planetary physiology, the study of solar radio bursts and coronal mass ejections, heliospheric and interstellar medium mapping, and studies of the early universe. Accessing this frequency range requires instrumentation above the Earth's ionosphere and thus collections of data must be accomplished in space.

In this paper, we propose a CubeSat science payload consisting of a deployable vector sensor antenna optimized for the 1 to 30 MHz frequency range. The six elements of the antenna enable complete measurement of the E- and B-field of incoming radiation at a single point in space. The complexity of a vector sensor is justified by an increase in sensitivity and the ability to mitigate terrestrial noise, which provides the potential to operate in lower-cost low earth orbits. A key aspect of the antenna is to provide the needed sensitivity in a small stowed volume. This is achieved with a vector sensor that measures 4m tip-to-tip and only occupies a stowed volume of 1U.

INTRODUCTION

The low frequency end of the electromagnetic (EM) spectrum (below 15 MHz) is one of the least explored windows in observational astronomy. Observations at these frequencies offers insight into a wide range of non-thermal astrophysical processes as well as highly redshifted thermal processes [1]. Applications within the solar system include observations of solar coronal mass ejections (CMEs) and associated plasma waves and solar radio bursts as well as planetary magnetospheres and their interaction with the solar wind and space weather. Beyond the solar system, low frequency radio observations will enable mapping of the local interstellar medium (ISM) and perhaps the detection of exoplanetary magnetic fields in the solar neighborhood. Finally, low frequency observations that probe very high redshifts open a window into the cosmological Epoch of Reionization (EoR) and the birth of the first stars and galaxies.

This material is based upon work supported by the Assistant Secretary of Defense for Research and Engineering under Air Force Contract No. FA8721-05-C-0002 and/or FA8702-15-D-0001. Any opinions, findings, conclusions or recommendations expressed in this material are those of the author(s) and do not necessarily reflect the views of the Assistant Secretary of Defense for Research and Engineering.

Ground-based observatories including LOFAR [2], LWA [3], [4], MWA [5], and the proposed SKA-Low [6], [7] are improving access to the radio sky down to about 20 MHz, but these telescopes are fundamentally limited by the ionospheric cut-off frequency and experience significant ionospheric distortion even at higher frequencies due to scintillation and severe time-varying refraction. The ionospheric cut-off frequency is the plasma frequency of the ionospheric peak, typically between 3 and 12 MHz, which is highly dependent on ionospheric conditions. Observations below the local plasma frequency are simply not possible from the surface of the Earth. In order to push to lower frequency observations, it is necessary to observe from space. A very limited number of observations in this frequency range have been conducted with no interferometric space missions to date.

The advent of CubeSats has changed the landscape and increased the feasibility of a multi-spacecraft interferometric array. Such arrays have been proposed (e.g. [8-10, 14-16]) and are a key step to lowering mission costs. It is still critical, however, to minimize the number of spacecraft required for such an array in order to keep costs and logistics reasonable. In [44] we described use of a vector sensor antenna rather than the crossed dipoles typically used for ground-based low frequency interferometric arrays or the tripole antennas

(dipole triads) often considered for space based arrays. The sensitivity advantage provided by the vector sensor is intended to reduce the number of spacecraft needed for mapping the sky below 15 MHz. The use of the vector sensor to provide characterization and mitigation of strong interfering sources also opens the possibility of making astronomically useful observations much closer to Earth than previously proposed missions, which often select Lunar orbits [13] or surface installations to exploit the radio shadow of the Moon [1]. In this paper, the focus is on the vector sensor payload including the desired data to be collected, and predicted performance, mechanical deployment, and the risk reduction activities that have occurred as we prepare this concept for operation in space.

This paper describes a CubeSat science payload consisting of a deployable vector sensor optimized for the 1 to 30 MHz frequency range, the low noise receiver front end, optimized for preserving the signal-to-noise ratio of the electrically-small vector antenna and the receiver digitizer and signal processor. The band of 1 to 30 MHz overlaps the radio sciences high frequency (HF) band, which is normally defined as 3 to 30 MHz. The vector sensor antenna occupies a volume of 1U (10×10×10 cm) when stowed and the multi-channel receiver front end and signal processor another 0.3U. When deployed, the vector sensor measures 4m tip to tip. The low noise amplifier (LNA) front end for the HF band is challenging due to the high dynamic range needed and the low power consumption requirement for operation in a small satellite. A design has been generated that has been optimized for this application. The mechanical and electrical designs for the deployable vector sensor are described and initial test results from the antenna and LNA are discussed. The challenge of the wide bandwidth, multiple receiver channels and limited downlink bandwidth is discussed and the proposed approach to implementing the science payload is presented.

SCIENCE DATA

In this section the science data products that are needed are explained. The focus of the payload is to collect these data with sufficient sensitivity and accuracy.

Calibrated radiometric

The science investigations described above require an imaging interferometer. In order to perform interferometric imaging, each spacecraft that makes up the interferometer collects time-synchronized data simultaneously. The recorded raw voltages from each channel on each spacecraft are cross-correlated either on the ground or in space. In this paper, we focus on ground-based cross correlation. In theory, interferometric data can be well calibrated using only astrophysical sources with known fluxes. In practice, however, the ability to inject calibration signals into the receivers onboard each spacecraft will make accurate calibration easier (see later discussion on Calibration Strategy).

Polarimetric

Polarimetric imaging at low frequencies is rarely done with ground-based instruments due to the challenge of disentangling ionospheric Faraday rotation from source polarization. This is further complicated by the ionospheric multipath caused by ordinary and extraordinary mode splitting and multiple layers common in low frequency ionospheric propagation [36]. A space-based interferometer composed of vector sensors would have two advantages when compared to ground-based instruments. First, Faraday rotation is significantly reduced due to the lower density plasma environment above the ionospheric peak. Second, each individual vector sensor has the ability to fully determine the polarization of incoming radiation in a single measurement. This feature will allow for new approaches to polarization calibration using data from each individual spacecraft in addition to aggregate interferometric data.

Ground-based interferometers typically collect two outputs representing orthogonal polarizations from each antenna (R/L for circular feeds, X/Y for linear feeds). The cross correlation process produces four correlation products (e.g. RR, RL, LR, LL). Each vector sensor interferometer member, which is composed of 6 elements, will produce six raw voltage outputs. Each cross correlated baseline will therefore have 36 correlation products. The inherent redundancy in these correlation products may prove useful in identifying and eliminating poorly calibrated antennas or individual channels. After the cross correlated data is calibrated, full Stokes (I, Q, U, V) images [37] can be generated.

Constellation relative positions

The image quality and angular resolution that an interferometer can provide depends on the values and diversity of baseline lengths and orientations. The longest baseline sets the angular resolution of the array in the same way that the diameter of an optical telescope sets its diffraction-limited angular resolution. Since each baseline samples a specific spatial Fourier component of the sky, diversity in baseline length and orientation improves the interferometric point-spread function (PSF) by sampling many spatial frequencies.

In space, baselines need not be limited to a 2D plane as they are for most interferometers on the Earth's surface. A space-based interferometer with members in a quasi-

random spherical 'cloud' formation ensures high baseline diversity and a correspondingly clean instrument PSF [11]. A variation using an ellipsoidal cloud rather than a spherical cloud was proposed in [10].

There are both minimum and maximum useful baseline lengths. The minimum useful baseline is set by the wavelength of the highest frequency at which the array operates. The minimum useful baseline is typically set at 10 wavelengths; for 30 MHz this provides a minimum separation of 100m. The maximum useful baseline is set by the scattering properties of the interplanetary medium (IPM) and interstellar medium (ISM). The medium effectively sets the maximum achievable angular resolution, so longer baselines will not improve imaging resolution. Reference [1] describes the scattering limits for the IPM and ISM for a range of frequencies. The maximum useful baseline for the vector sensor array is set by the scattering limit at lower end of the frequency range. The scattering limit of the IPM at 3 MHz corresponds to a baseline of about 100 km. Baselines longer than this upper limit would improve angular resolution at higher frequencies, but the maximum baseline length is set assuming that broadband imaging across the full band is desired.

The positions of each spacecraft relative to every other must be measured to a precision of ~1/10 of the shortest operating wavelength to minimize phase errors. Since the highest operating frequency of the vector sensor interferometer is 30 MHz, 1m relative accuracy in position knowledge is sufficient.

Individual satellite orientation

Knowledge of the orientation or attitude of each spacecraft is required in addition to relative position knowledge. Each individual vector sensor requires attitude knowledge so that the varying voltages on each element can be correctly interpreted into direction of arrival information. Similarly, the interferometry requires that each member have attitude knowledge so that baseline orientations and polarization can be calculated correctly. Miniature star trackers on each spacecraft will be the nominal attitude sensors. Since the vector sensor is effectively omnidirectional, active attitude control is not required as long as the rotation rate of each spacecraft either does not change significantly, or if the data is transformed into a common rotational frame. With the vector antenna we choose to perform the transformation into a common reference. This can be accomplished without loss of information with a vector antenna sampling the full electromagnetic field. In contrast, triad antennas must maintain tighter on-orbit stability, since they do not completely sample the electromagnetic field and thus a transformation of coordinates cannot be accomplished without loss of information.

Data Downlink

When in wideband observing mode, the science receiver system in each spacecraft will directly sample the full band. Assuming a Nyquist sampling rate with a 33% margin (80 Msamples/second for 30 MHz maximum frequency) and 14 bit samples, each spacecraft will generate 6.7 Gbits/second. The raw science data volume rate will be reduced through decimation in frequency or time, partial processing in space, and pre-whitening followed by scaling and bit depth truncation.

Figure 1 illustrates the science data flow from collection by the antenna to dissemination for science data product generation. After the antenna signals are converted to digital in the analog-to-digital convertor (ADC), the signals are passed to a software-defined radio where the digital signals are converted to baseband through a digital in-phase/quadrature (DIQ) conversion. Shown in this figure are two fundamental observational interferometer modes: wide-band snapshot collection and narrow-band collection. The data after DIQ processing will cover the full band from 1 to 30 MHz, but collection at that rate cannot be sustained for long periods of time due to the relatively lower downlink rate and finite onboard storage. Only snapshots in time can be collected and these collections can be synchronized across the constellation. Longer duration observations will be performed in the narrow-band mode to reduce data accumulation. In this mode the baseband data are passed through polyphase filter bank where specific bands of interest are selected. Pre-whitening allows for bit depth reduction since the transformation reduces the dynamic range without significant loss of information content.

On-board data is buffered, error correction codes (ECC) are applied and the data downlinked to a ground station and buffered on a server. The downlink data will be transmitted over a science data network where error correction decoding, calibration and pre-processing to remove the whitening transform is applied. These data are then disseminated for analysts to perform more detailed scientific investigations.

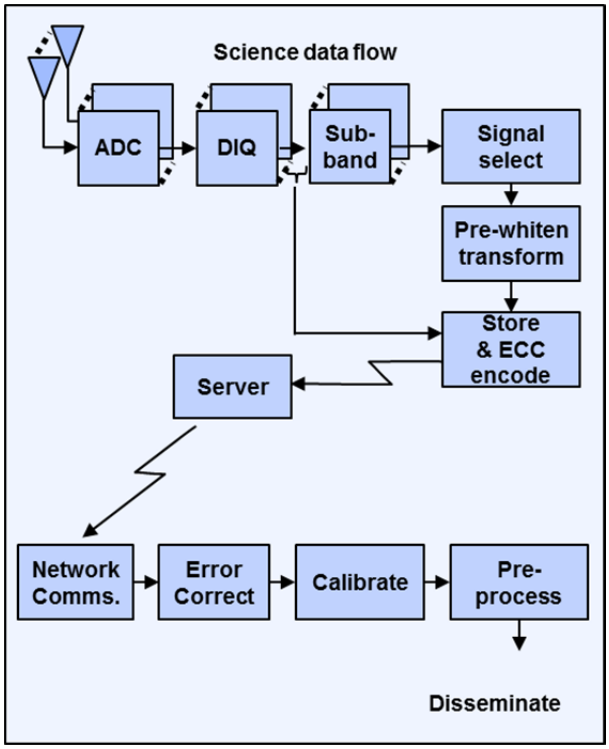

Figure 1. Science data flow from the CubeSat antenna elements through the payload receiver, signal detector and storage prior to downlinking data. The initial steps in ground processing are shown in the lower part of this figure.

To generate the interferometric results there are two options for cross-correlation of the raw voltage data: in-space distributed correlation or correlation on the ground (raw data downlink). In-space distributed correlation has been proposed as a means to reduce the total data volume that must be downlinked to the ground (e.g. [12]), especially in cases where the space-based interferometer is very far away from the Earth and has a highly constrained downlink budget. In-space correlation requires the exchange of large data volumes between all of the spacecraft that form the interferometer, but reduces the data volume to be downlinked since the correlated products are averaged and only the averages are sent to the ground. The second option for correlation is to downlink raw voltage data directly to the ground and then correlate as depicted in Figure 1. This option becomes feasible when there is a larger link budget available to the spacecraft in the constellation, either because they are closer to Earth, have high-gain communications systems, or have access to large aperture ground stations.

There will be unwanted radio noise sources that must be filtered out even when observing from above the Earth's ionosphere. The Earth's ionosphere will block most terrestrial radio signals below the ionospheric cut-off frequency, but some may leak out through ducting or other mechanisms. Higher frequency terrestrial signals will also pass through the ionosphere unimpeded. The Earth's natural auroral kilometric radiation (AKR) is also a powerful noise source when attempting to observe astrophysical or solar system objects. These unwanted noise sources can be reduced or removed in three ways: 1) increasing the distance between the Earth and the interferometer, 2) placing a solid object like the moon between the interferometer and the Earth, or 3) by using spatial filtering to de-weight signals originating from the Earth. Previously proposed space-based low frequency interferometer approaches have opted for one of the first two strategies, either placing the interferometer at a Lagrange point or in a distant retrograde orbit or by using the shadow of the moon to block noise from the Earth. The vector sensor interferometer will use the third approach. The ability of the vector sensor to measure the full EM wavefield naturally infers the ability to place beam pattern and polarization nulls in specific locations. Steering a null in the direction of the Earth will offer significant attenuation of signals from that direction [18]. This pre-whitening transform capability will allow the vector sensor interferometer to operate much closer to the Earth than previously proposed systems, allowing for significantly increased data downlink volume.

As noted previously, the vector sensor data can be transformed into a common galactic coordinate system. This transformation of coordinates can be incorporated into the pre-whitening transform. Because the vector antenna measures the full electric and magnetic fields it provides an algebraically complete representation of the electromagnetic wave field as observed at the CubeSat. Because this is a complete representation we can we can perform a rotation of the data collected by each spacecraft into a common galactic reference frame without loss of information. We note that a tripole antenna does not provide a complete representation of the electromagnetic field, so lossless transformation on board the satellite into a galactic reference frame is not possible.

SCIENCE PAYLOAD DESCRIPTION

A critical aspect of the science data collection is to collect sky-noise limited measurement of RF signals in the HF frequency range from space. An HF antenna and receiver system is required that can be implemented on a satellite platform and interferometric constellations of receivers are desired to enable meaningful angular resolution. Determining the specific antenna to be used for low frequency mapping requires an overall system tradeoff between complexity on a single spacecraft and

system complexity in moving data between different nodes or to the ground. Interferometric aperture synthesis imaging requires the signals from each antenna be combined at a central location so the communication problem quickly grows as the number of receiving nodes increases. Measurement of source wave polarization state and the avoidance of antenna pattern nulls suggest that, at a minimum, each node should have a tripole antenna. Using an HF vector sensor, we consider increasing the complexity of each node from the minimum tripole to reduce overall system complexity and cost.

The use of vector sensing is motivated by the following observations:

1. Vector sensors are able to determine direction of arrival of sources [19,20] without resorting to multiple orientations or poses as required for a triad.

2. Vector sensors maximize the cross-correlation statistics collected from a single point in space to the limit allowed by the fundamental nature of the EM fields [26]. This maximizes the utility of a single satellite short of deploying a spatially distributed array and will provide a more capable interferometer with fewer spacecraft. While the final constellation is expected to contain multiple satellites, the ability to collect these statistics with a vector sensor allows radiometric imaging to be performed with a single spacecraft.

3. Vector sensors allow an antenna system to null or isolate specific sources [18]. This potentially is of benefit in the near earth environment where natural and man-made signals can effectively mask weaker phenomena and drive very high dynamic range requirements in the RF data collection and signal processing.

A block diagram of the antenna, vector antenna modeformer and receiver is shown in Figure 2

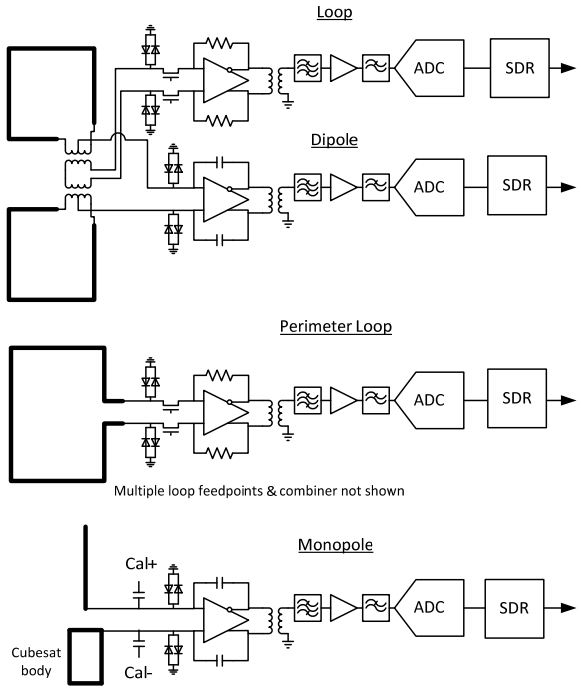

Figure 2. Antenna and receiver block diagram showing the signal path through the software defined radio (SDR). One of two loop/dipole elements is shown along with the perimeter loop and monopole element.

Vector Sensor Antenna

An electromagnetic vector sensor (EMVS) [20] samples the electric field *E* and magnetic field *H* (or magnetic flux density *B*) at a single location in space and with a common phase center. To do this, a vector sensor is composed of three orthogonal dipole elements and three orthogonal loop elements. These six elements allow for a complete measurement of the E-field and B-field amplitude and phase of incoming radiation as well as calculation of the covariance terms between these components. The vector sensor is named for its capacity to fully measure the electromagnetic vector field rather than the single scalar measurement associated with a single element antenna. One consequence of sensing the full E and B vectors is that the vector sensor natively measures full polarization information.

Our implementation of a full 6-mode vector sensor on a CubeSat utilizes effectively two crossed vertical wire loop antennas, two crossed horizontal dipole antennas, a vertical wire monopole antenna, and a horizontal loop antenna as shown in Figure 3. Dual mode loop-dipole elements are described in [27,31,32]. The 10 MHz radiation patterns of the six modes are shown in this figure. The wire length of the antenna arms is chosen in the range of 1.5m to 2m and keeps the antennas electrically small, below resonance, so that constant

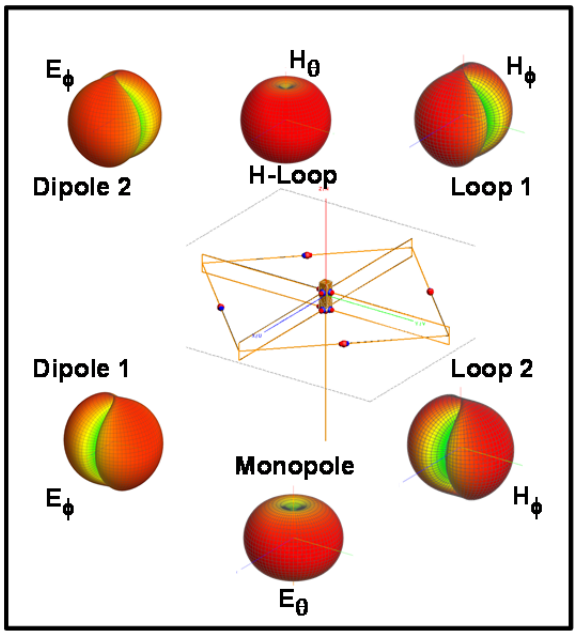

Figure 3. Gain patterns of the different antenna elements forming the vector sensor antenna.

radiation pattern shapes are maintained over the desired frequency range as depicted in Figure 4 for a 3m tip-to-tip antenna. Simulations show that the antenna size can be increased to at least 6m tip-to-tip without significant degradation of the antenna element patterns. The four modes associated with the two crossed wire loop antennas and two crossed horizontal dipole antennas are generated by sum and difference modeformers [27]. The horizontal wire loop antenna has four feed points, which enables uniform current on the wire and constant radiation pattern shape over wide bandwidth. The vertical wire monopole has a single feedpoint counter-balanced by the CubeSat metallic body.

A key performance metric of the vector antenna is that the measurements from each of the antenna elements are dominated by external sources rather than by internal thermal noise due to electronic components. This metric is normally accomplished by maximizing the size and the resulting effective height of the antenna subject to constraints on stowed volume, mass, and frequency independence of the element patterns. The International Telecommunications Union (ITU) provides a model of galactic noise [23] is used in the analysis below.

The ITU model predicts galactic noise, integrated over all directions, is approximately 15 dBnV/m/Hz^{½} at 5 MHz. Typical high dynamic-range radio front ends with good protection from static discharge typically provide performance of about 5 dBnV/Hz^{½} when referenced to

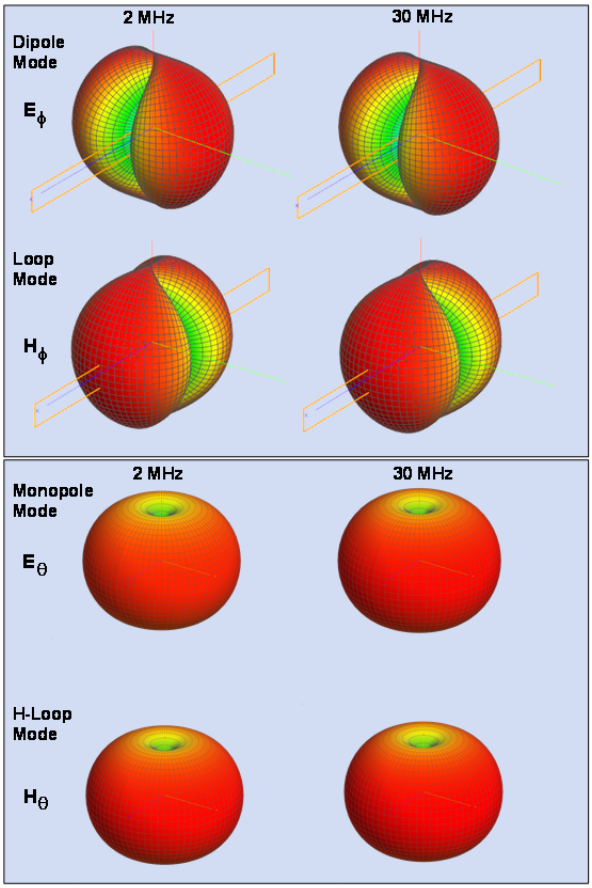

Figure 4. Simulated element patterns showing that the gains are nearly independent of frequency.

the antenna input port. To ensure that external noise dominates, an effective antenna height of at least 1 m is required (5 dBnV/Hz^{½} <<(15 dBnV/m/Hz^{½}*1m = 15 dBnV/Hz^{½}). Since the effective height of an electrically unloaded dipole is half the physical length, a minimum antenna length of 2m is required. This is one alternative approach to small receive system design. Often the antenna performance is analyzed based on the effective aperture [1], but for electrically small antennas it is difficult to electrically match for power transfer. By analyzing the equivalent circuit for voltage response we avoid concerns with impedance mismatch. We note that while the ITU model assumes omnidirectional sources, we are interested in determining the variation of intensity with direction.

As built, the prototype loop/dipoles are 4m tip-to-tip, the monopole is 2m long, and the area of the loops is 8 m^2 for the horizontal perimeter loop and 0.8 m^2 for the two vertical loops. Increasing the size of the elements would increase their effective height. With the current size the element radiation patterns are nearly frequency-

independent, which simplifies calibration and processing.

Calculation of the element gain and achieving maximum signal-to-noise ratio (SNR) from an electrically small antenna necessitates a good model for the antenna elements. The equations for effective height and impedance of short dipole and loop are as follows:

The effective height of a dipole that has a triangular current distribution with length $l$and wire radius a is

$$h_e(\theta,\phi) = \frac{l}{2}\sin\theta, \tag{1}$$

and with a real radiation resistance [38] of

$$R_r = 20\,\pi^2\left(\frac{l}{\lambda}\right)^2. \tag{2}$$

For the uniform current loop with area A and N turns the effective height is

$$h_e(\theta,\phi) = j\frac{2\,\pi N\,A}{\lambda}\sin\theta, \tag{3}$$

and with radiation resistance of [46]

$$R_r = 80\,\pi^2\left(\frac{NA}{\lambda}\right)^2. \tag{4}$$

These equations are used in the optimization of the receiver and antenna interface described later.

CubeSat Vector Sensor Deployment

A deployment demonstrator for a CubeSat vector antenna has been designed and built. The CubeSat vector antenna uses metal carpenter's tape booms and wires to form two orthogonal dipoles, a monopole, and three loops. The entire antenna coils up around a central hub that fits into 1U as shown in Figure 5 (a) and Figure 6. In Figure 6, the deployed prototype is shown in a gravity offloading test frame. This frame is needed so that the deploying tapes do not drag on the ground.

The CubeSat antenna prototype deploys in two stages. First, the two tape coils are separated by a telescoping column (Figure 5 (b), Figure 6 top). The telescoping action is driven by a compressed spring. Second, the tape coils are released to unroll under their own power (Figure 5 (c), Figure 6 bottom). No motor is needed due to the strain energy stored within the coiled tapes. The unrolling tapes pull out the perimeter loop wires, which are wrapped on a spool when stowed as shown in Figure 6 top. The metal tapes themselves serve as the electric current conductor for the four loop/dipole antenna elements. The horizontal perimeter loop is fed by four balanced twisted-pair wires extending back to the central hub.

The current prototype was made from off-the-shelf steel carpenter's tapes and 3D printed ABS plastic components. The as-built prototype with 2m long tapes has a mass of approximately 1 kg. The steel tapes are the major contributor to the antenna mass. The steel tapes could be replaced with composite tapes with a conductive layer to save more mass. If the ABS components were designed to be made of aluminum with minimum mass, the total mass of the system would not grow significantly.

The antenna deployment was very repeatable for 1.5m long tapes. When deploying with 2m long tapes the gravity load along the mid-span of the tapes would sometimes cause one or more tapes to buckle before full deployment was complete. In zero gravity this buckling effect would not be an issue.

Items that still need to be addressed in the design include: considering the effects of on-orbit loads and whether they would cause buckling of the deployed tapes, ensuring proper tension in the perimeter loop wires without causing buckling of the tapes and stowing the perimeter loop wires to ensure that no snagging occurs during deployment. Several solutions to these

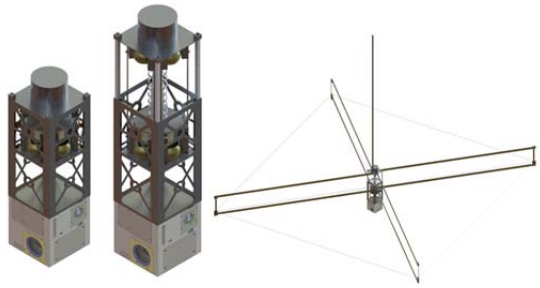

(a) (b) (c)

Figure 5. Vector Sensor payload design. The 3U CubeSat with the vector antenna fully stowed is shown in (a), the CubeSat with the antenna section telescoped but antenna stowed in (b), and the CubeSat with the antennas completely deployed in (c). Note the thin horizontal loop around the deployed vertical rectangular tape spring elements in the fully deployed image. The sixth element of the vector sensor is the monopole extending upward from the CubeSat body.

outstanding items have been proposed and will be considered as development continues.

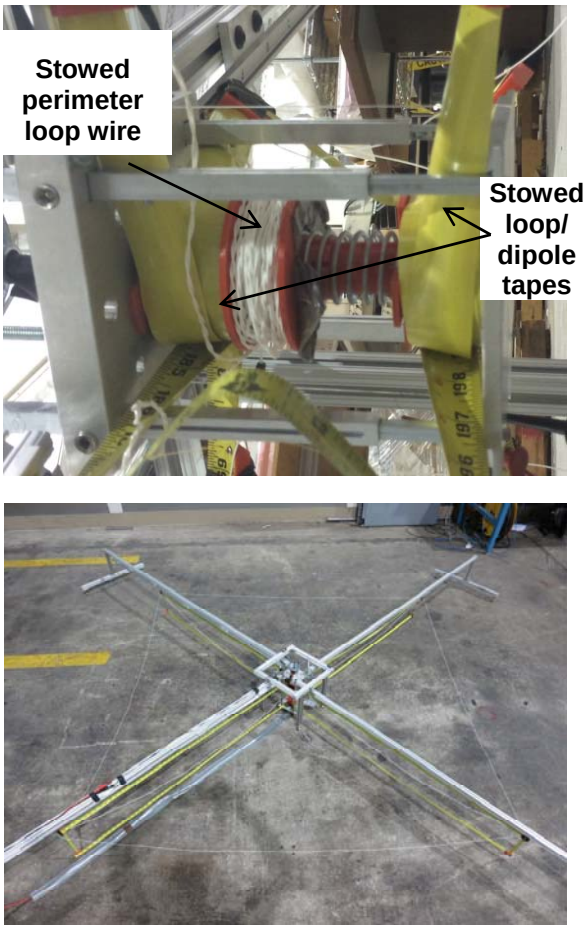

Figure 6. Stowed (top) and deployed (bottom) prototype CubeSat vector sensor. A gravity offload system was used to prevent the tape spring elements from buckling during deployment. The monopole is not shown in this image. The third loop element is composed of wire supported by the tips of the deployed tape loops/dipoles and is parallel to the ground in the above image.

Receiver System

The receiver system provides low noise amplification, antenna loop/dipole mode forming of sum and difference modes, calibration injection, electrostatic and EMI protection, filtering, analog-to-digital conversion, digital filtering and signal selection and baseband processing.

Referring to Figure 2, this particular antenna system consists of electrically small split loops, fed at two points, which may be separated into loop and dipole modes. Given the highly reactive and low real resistance of the antenna impedance of these two modes, traditional Foster type impedance matching is impossible to achieve over wide bandwidth. We have implemented non-Foster matching circuitry, which for the dipole elements is similar to those shown in [29, 30, 33], and for the loop mode we use our own design. The result is that we are able to preserve the antenna loop and dipole SNR over a wide fractional bandwidth.

The loop and dipole modes are separated by means of center tapped transformers connected to the two halves of the split loop. The center taps separate the common mode current in each half loop and send it to the dipole mode amplifier. The secondary windings are connected together and send the differential mode currents to the loop mode amplifier.

The loop mode of the antenna appears electrically to the low noise amplifier as a voltage source in series with an inductance. Since effective height of a loop increases with frequency (Eq. 3), this voltage increases with frequency. This increasing voltage is counteracted by the increasing inductive reactance, resulting in a nearly constant current over frequency. It naturally follows that a transimpedance amplifier would be the correct solution as the stage to match to the loop mode. [29] Because the transimpedance amplifier holds its input at virtual ground, the effect of parasitic capacitance is negated and no resonance effects are seen as they are with other active matching configurations.

The loop mode amplifier is presented with a very low impedance at its input port. In typical transimpedance amplifiers, this low impedance effectively negates the feedback path, causing noise gain peaking up to the amplifier's open loop gain in the worst case. Grubb [29] uses a transformer to step up the antenna impedance to avoid noise gain peaking at the expense of sensitivity. The negative consequences of the noise gain peaking is avoided in our approach by the use of a common gate current buffer before the operational amplifier. In the low impedance case, the common gate amplifier becomes common source relative to the feedback path, and only the small thermal noise on the gate of the very low noise transistor is amplified through the amplifier noise gain mechanism.

The dipole mode consists of a voltage source in series with a small capacitance. The voltage will remain constant over frequency due to the effective height being constant. Since this capacitance is very small, any parasitic capacitance will act as a voltage divider. Again, it naturally follows that a charge amplifier is the correct solution to negate the effect of parasitic capacitance and provide flat gain over frequency [29,30].

The analog paths of the payload require calibration injection to ensure that absolute calibration of the amplifier chain is maintained. This is accomplished by injecting a small calibration current through a large resistor for the loop mode, and a small capacitor for the dipole mode. The resulting mode-formed signal and calibration is then filtered through an AM and FM broadcast band reject filter and passed through a second stage of amplification before the analog-to-digital converter (ADC). The ADC is connected to an off the shelf Xilinx Zynq-based CHREC processing board [34] where the data is processed and compressed before downlinking to the earth.

The CHREC processing board has been tested for radiation tolerance by the developers and provides a moderate level of computational capability. The software defined radio algorithms are computational high so significant optimization will be required to map them onto the CHREC processing board.

Calibration strategy

Calibration consists of verifying all the factors that are required to generate accurate measurements of electromagnetic radiation as a function of angle. The goal is to determine levels that are traceable to the National Bureau of Standards (NBS) with a known uncertainty. To achieve this level of calibration requires measuring and calculating parameters of individual satellites as well as an understanding of the uncertainties associated with interferometry impacts the resulting radiometric calibration. In this section we consider two aspects of that calibration, individual satellite radiometric calibration and the closely related antenna-to-antenna gain and phase matching.

Calibration starts with ground measurement of components and the end-to-end system which necessarily includes element pattern measurement. A portion of these measurements will be performed in the Lincoln Laboratory RF Systems Test Facility and end-to-end system and antenna measurements will be undertaken on the final antenna and receiver design prior to launch by testing in a near-field scanning facility similar to the SPAWAR San Diego pattern measurement range [25]. Effective height calculation and loss analysis of the electrically small loops and dipole responses is straightforward and factors significantly into the radiometric calibration. Ground measurements will verify those calculations. The Lincoln-Laboratory facility is able to generate NBS-traceable measurements. These ground measurements will verify the stability of the instrumentation over time, temperature and operating conditions.

On-orbit internal calibrations will be used to verify the receiver gain and noise levels during normal operation. A stable, National-Bureau of Standards (NBS) traceable calibration sources will be injected into the six antenna inputs on each satellite to provide an accurate power reference [24,29]. A decision on whether this signal is switched or coupled into the input has not yet been made. Figure 2 illustrates capacitively coupling the calibration source. The injected signal will serve as both a precision reference level as well as a source that can be used to measure element-to-element or, more accurately receiver channel-to-channel gain and phase differences as a function of frequency. The source will be a combination of a calibrated noise diode and from a calibrated comb generator as is often done for precision instruments [39]. This coupled input allows on-orbit tracking of element-to-element (i.e. receiver channel-to-channel) passband amplitude and phase responses, and also allows the overall phase response of the receivers to be referenced to GPS timing so that satellite-to-satellite interferometry can be accomplished more precisely. Calibration signal injection will be under program control and will be turned off during normal data collections.

A final calibration check is to verify the performance with external sources such as Cas A, Cyg A or Vir A as they provide both a spatially point-like source and have relatively well-known spectral intensities. In addition to comparing the source intensity to other measurements that have been made by ground-based instruments at the upper end of our operating band, these sources provide a verification of the vector sensor element patterns and channel-to-channel gain and phase. The vector sensor is a unique antenna in that the response of a calibrated antenna to the electromagnetic field of the sky is invariant to first order under rotation. This invariance allows for the correction of angle-dependent element gain patterns and will serve to characterize second order effects by looking at residuals between calibration data and the calibration model.

For an interferometric constellation of vector sensors we intend to use satellite-to-satellite closure phase to further resolve and verify phase and amplitude calibration as a function of frequency. This requires joint interferometric processing of low level data from the satellites.

Self-Interference

Self-interference of the satellite with the HF vector sensor is a significant risk. Switching power supply noise from solar power voltage regulators and DC/DC converters is the most likely source of interference. It is necessary to prevent this noise energy from being conducted into the receiver or re-radiated by the solar

panels or spacecraft structure into the vector antenna. Previous high-performance designs have used multiple techniques to control noise. These include local shielding, bypass filters, triaxial shielded cables for power and signal paths, isolation of grounds and power supplies and physical separation. Steps will be taken to implement these steps within the mass, time and cost constraints of the development program. The final step is to accept that there are some noise sources that will not be controlled. In those cases the noise spectrum will be controlled and characterized so that it is constrained to a band not of interest. This constraint is commonly accomplished by frequency locking of various clock oscillators, power supply switching frequencies, etc. with the intent to constrain the degraded frequencies to a very narrow band. Implementation of this approach often requires moving away from commercial-off-the-shelf components.

TESTING

Development of subsystems to demonstrate the vector sensor is underway. A full test of the vector sensor's capabilities requires spaceflight in order to access the galactic sky below 15 MHz. Prior to that we have been maturing the concept and technology through ground-based testing augmented with high altitude balloon-based testing to mature the antenna concept.

Ground based testing

A rugged electromagnetic vector sensor for ground-test use in the HF band (1-30 MHz) has been implemented based on the design of [32]. Two copies, designated Atom 1 and Atom 2, have been fabricated to enable basic interferometric experiments. The vector sensor design used for ground-based testing is composed of three orthogonal rings approximately 1m in diameter (Figure 7). Each of the rings has two ports that are connected to a sum and difference hybrid. The result is that each physical loop serves as both a dipole and a loop [31, 32]. The full antenna produces the six output channels consistent with measuring each component of the electromagnetic field, referenced to the orientation planes of the three loops. For the space-based application, a different mechanical design (but similar electrical design) is needed in allow the antenna to stow and then deploy from a spacecraft as shown in Figure 5.

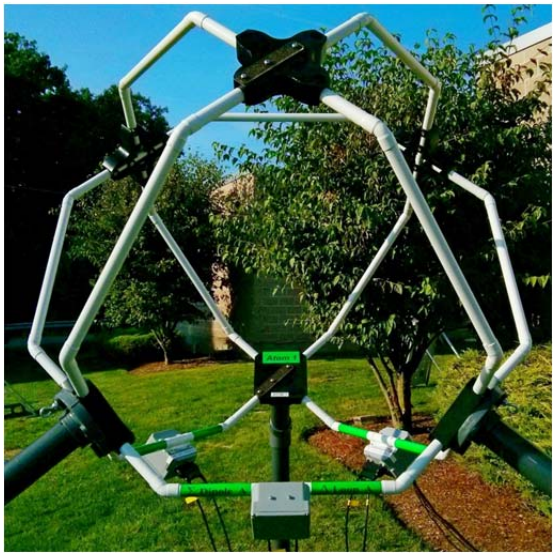

Figure 7. Atom 1 vector antenna at MIT Haystack Observatory. The three octagonal loops that form the vector sensor are painted copper tubing and the support posts are PVC. Each loop is 1m in diameter. This vector sensor is intended for ground testing only.

Test Plan Description

Ground-based testing consists of separate measurement campaigns for terrestrial and extraterrestrial sources to assess the sensor and algorithm capabilities. Terrestrial sources that are being used for testing include the NIST WWV broadcasts at various frequencies [35], over-the-horizon radar signals from the MARACOOS HF radar network [35], and a locally-controlled HF transmitter. Applying our vector sensor imaging algorithm [26] to these terrestrial signals allows verification of the algorithm's direction-finding capabilities with single and multiple sources. Extraterrestrial sources that will be used for testing include solar radio bursts and strong galactic sources like Cas A or Cyg A. These signals will allow us to verify the imaging capabilities of our vector sensor algorithm. Further testing including remote deployment and interferometric imaging with multiple vector sensors are planned pending the completion of the local testing campaign.

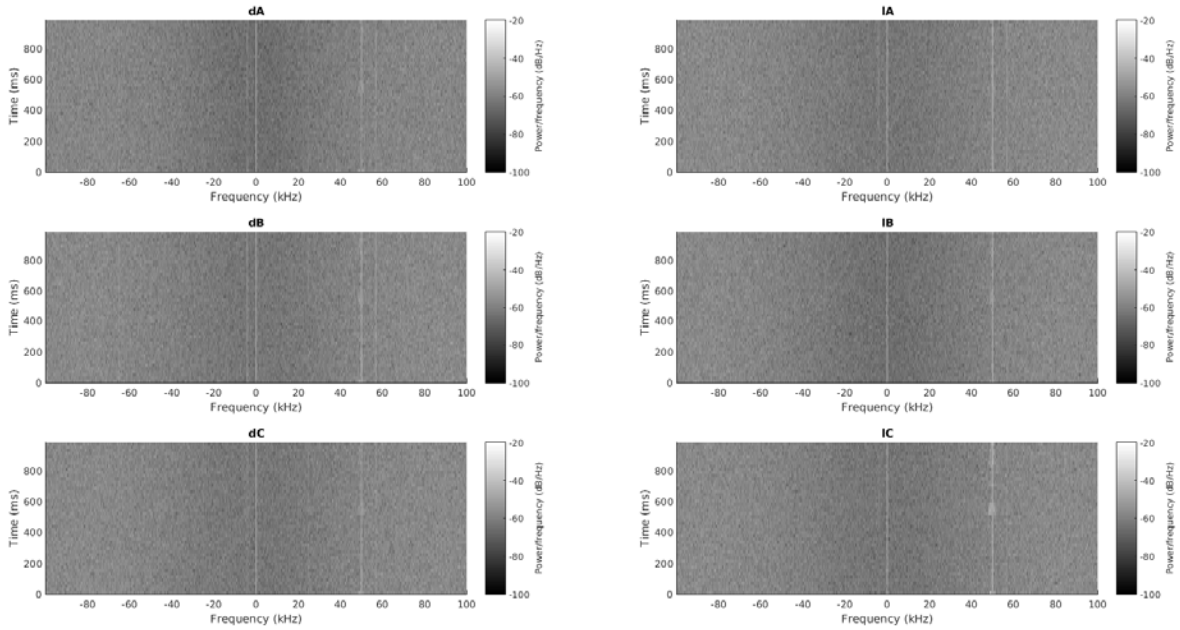

Figure 8. Spectrograms from each Atom element (top). The left column spectrograms are from the dipole elements and the right column spectrograms are from the loops. Frequency is on the x-axes and time increases upward on the y-axes of the spectrograms. This measurement is 200 kHz wide and centered at 14.95 MHz. The WWV signal is clearly visible at +50 on the horizontal scale in the spectrograms. The signals at DC in each of these plots are a receiver artifact.

Initial Results

Initial testing of the Atom 1 and Atom 2 vector antennas is in progress at MIT Haystack Observatory in Westford, MA. An initial test was the detection and mapping of the NIST WWV transmission. Figure 8 shows spectrograms from each element of Atom 2 relative to the tuned frequency of 14.950 MHz. Figure 9 illustrates an image produced from the same data using an equal area discretization on the sphere [22] and the maximum-likelihood estimation algorithm of [26]. The results presented here are preliminary, but do indicate that the vector sensor is functioning properly and is able to localize bright sources.

MIT Haystack Observatory is relatively close to Boston, MA, so the strongest ambient signals are man-made. Noise characterization for the full system is underway but is impaired by the local noise sources. Testing at the radio quiet Owens Valley site should allow for improved understanding of the receiver system performance as well as providing data that can be used for sky imaging at frequencies above the ionospheric cut-off.

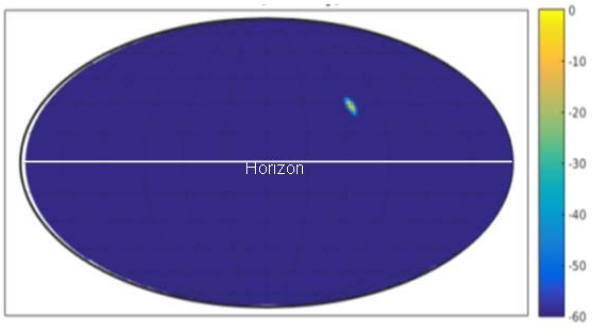

Figure 9. Example of direction finding for reception of the WWV radio transmissions at 15 MHz (the line at +50 kHz in Figure 8). The source map coordinates are local elevation and azimuth, with 0 degrees in elevation, the local horizon, marked by the white line. The color indicates the Stokes intensity, I, in dB.

Balloon based testing and results

Ground-based testing of the vector sensor and receiver have demonstrated the efficacy of the overall approach, however to mature the concept further a high altitude flight test was planned and executed. The specific goals of this balloon-based testing were to mature the concept and some of the components, particularly the electrical model of the satellite antenna and demonstrate the vector sensor concept in a flight test at altitude with line-of-sight to emitters. In particular it was important to be away from the earth where mutual coupling and multipath changes the element responses.

Figure 10 illustrates the balloon vector sensor payload and receiver. The high altitude balloon payload consisted of a lightweight, low-power geolocation system with six receiver channels, vector sensor modeformer, digitizer, global positioning system (GPS) receiver, an inertial measurement unit (IMU)/inertial navigation system (INS), data recorder and battery along with other payloads including multiple video cameras. The train of payloads is shown in Figure 11 just prior to launch on the left and shortly after the launch on the right.

The vector sensor antenna used in the balloon flight consisted of 1.4x1.4m horizontal loop, dipole/vertical loop depth of 0.18m and vertical monopole element of 1m in length. The antenna dimensions were chosen for maximum overall loop areas, constrained by mass and stability limits. All components of the antenna were constructed of thin wire elements, stabilized by a network of Kevlar lines for stability at altitudes exceeding 26.5 km (87,000 ft) and the total mass of the assembly was 2.45kg (5.4 lb).

Pre-flight ground testing of the high-altitude receiver assembly was undertaken, including thermal, near-field probing and anechoic chamber testing prior to high altitude balloon flight testing. Ensuring the entire balloon payload train fit within FAA allowed limits, while ensuring stability under potential high wind loading were key concerns and thus extensive rigging testing was performed. This rigging is shown in Figure 13.

During the flight test the balloon and payload assembly experienced an ascent to 26.5 km at a rate of 7.1 m/s (1400 ft/min), prior to burst with data collection throughout the entire flight. A photograph taken from a documentary camera taken just prior to balloon burst is shown in Figure 12.

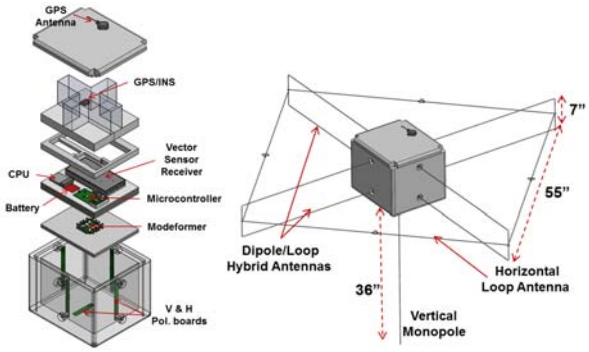

Figure 10. High-Altitude Balloon HF receiver assembly (with GPS/INS, data recorder and battery) and vectors sensor.

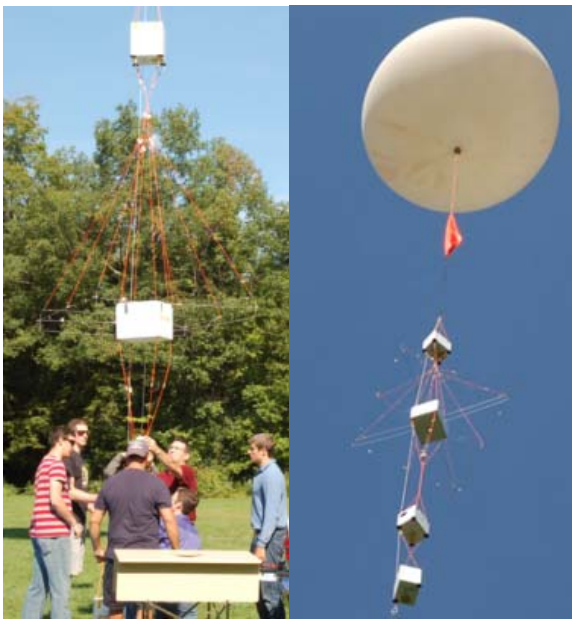

Figure 11. Preparing to launch the balloon (left) and a picture taken shortly after launch showing the telemetry, GPS, and vector antenna modules.

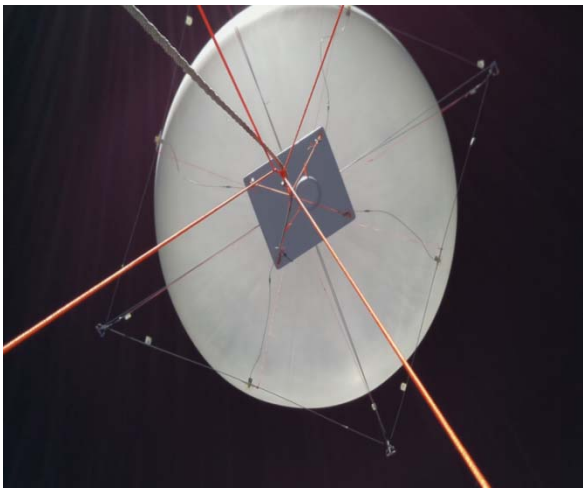

Figure 12. Vector sensor and receiver payload as seen by an up-looking camera just prior to balloon-burst at 26.5 km.

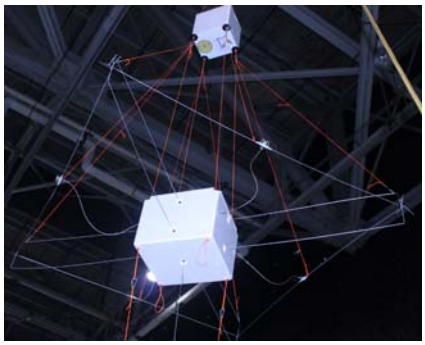

Figure 13. The completed receiver and vector sensor assembly shown during test preparation.

During the flight a reference source located at Hansom Air Force based transmitted a beacon signal at 12.15 MHz. The platform INS allowed a determination of the true azimuth angle to the source. Figure 14 illustrates that the true azimuth angle to the source agrees well with estimates of the angle of arrival generated from the vector sensor. The vertical axis in this figure is the azimuth angle in degrees relative to the platform reference and the horizontal axis is time. Due to rotation of the platform the azimuth to the source varies considerably as a function of time.

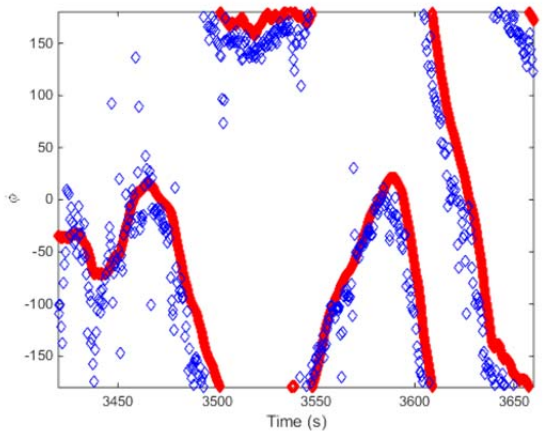

Figure 14. Vector sensor angle estimate (blue circles) tracks well with INS truth data (shown in red) for transmitting beacon in high altitude balloon test data.

When fully processed, the high altitude balloon test results demonstrate an angle-of-arrival estimate accuracy of ~3° (combined statistical and bias errors) for this particular design. The angle accuracy was limited primarily by the minimal system-level calibration that was performed prior to the test flight. In ground processing we found that the two loop modes from the loop/dipole elements suffered from low far-field gain. This was quickly corrected after the flight and a follow-on flight is expected to produce even more accurate results.

CONCLUSION

The low frequency portion of the electromagnetic spectrum (below 15 MHz) is poorly explored due to the opacity of the Earth's ionosphere at those frequencies and the need for large interferometric baselines to achieve useful angular resolution and sensitivity. A wide range of science topics would greatly benefit from measurements in this band, including magnetospheric planetary physiology, the study of solar radio bursts and coronal mass ejections, heliospheric and interstellar medium mapping, and studies of the early universe. Accessing this frequency range requires instrumentation above the Earth's ionosphere and thus collections of data must be accomplished in space.

In this paper, we propose a CubeSat satellites and a science payload consisting of a deployable vector sensor antenna that has been optimized for the 1 to 30 MHz frequency range. The six elements of the antenna enable complete measurement of the E- and B-field of incoming radiation at a single point in space. The complexity of a vector sensor is justified by an increase in sensitivity and the ability to mitigate terrestrial noise.

Mitigation of terrestrial noise creates the possibility of using lower-cost low earth orbits to collect the data. The simultaneous use of the CubeSat form factor and low earth orbit provides the potential for affordable space-based radio astronomy.

This paper describes the payload in detail from the vector sensor antenna that measures 4m tip-to-tip and only occupies a stowed volume of 1U to the receiver, calibration and initial signal processing. Of particular note is the use of pre-whitening to reduce the dynamic range of the collected data since that allows for a reduction in bit depth in the downlink to the ground station.

Prototyping and experimentation has significantly matured the vector sensor payload and antenna concept to where the next steps are to build and test form factored instruments that are capable of being space qualified.

ACKNOWLEDGMENTS

The authors would like to thank the MIT-LL Advanced Concepts Committee and Line programs for their support of this effort. The CubeSat vector antenna mechanical design and fabrication was provided by Richard Arnold and Alec Delaney. Fabrication of the Atom antenna was accomplished by Tom Alosso and Tom Matte. The team that conducted the balloon flight included participation from multiple Lincoln Laboratory Divisions, Peter Hurst led the payload integration, Larry Retherford led mechanical integration, Eric Phelps led analysis of the results, and David Patterson led the launch and recovery teams. Ground testing of the Atom antennas included significant efforts by Will Rogers, Tom Brown, and Alexander Morris. Thanks to Sara Klein for assisting with the project administration.

References

1. M. De Vos, A. W. Gunst, and R. Nijboer, "The LOFAR telescope: System architecture and signal processing," Proc. IEEE, vol. 97, pp. 1431–1437, 2009.
2. S. W. Ellingson, T. E. Clarke, A. Cohen, J. Craig, N. E. Kassim, Y. Pihlstrom, L. J. Richard, and G. B. Taylor, "The Long Wavelength Array," Proceedings of the IEEE, 2009. [Online]. Available: http://lwa.phys.unm.edu/docs/lwa0157.pdf. [Accessed: 17-Oct-2015].
3. G. Hallinan, "The Owens Valley LWA," in Exascale Radio Astronomy, 2014, vol. 2.
4. C. J. Lonsdale, R. J. Cappallo, M. F. Morales, F. H. Briggs, L. Benkevitch, J. D. Bowman, J. D. Bunton, S. Burns, B. E. Corey, L. deSouza, S. S. Doeleman, M. Derome, A. Deshpande, M. R. Gopala, L. J. Greenhill, D. E. Herne, J. N. Hewitt, P. A. Kamini, J. C. Kasper, B. B. Kincaid, J. Kocz, E. Kowald, E. Kratzenberg, D. Kumar, M. J. Lynch, S. Madhavi, M. Matejek, D. A. Mitchell, E. Morgan, D. Oberoi, S. Ord, J. Pathikulangara, T. Prabu, A. Rogers, A. Roshi, J. E. Salah, R. J. Sault, N. U. Shankar, K. S. Srivani, J. Stevens, S. Tingay, A. Vaccarella, M. Waterson, R. B. Wayth, R. L. Webster, A. R. Whitney, A. Williams, and C. Williams, "The Murchison Widefield Array: Design Overview," Proc. IEEE, vol. 97, no. 8, pp. 1497–1506, Aug. 2009.
5. C. L. Carilli and S. Rawlings, "Motivation, key science projects, standards and assumptions," New Astron. Rev., vol. 48, no. 11–12, pp. 979–984, Dec. 2004.
6. P. E. Dewdney, P. J. Hall, R. T. Schilizzi, and T. J. L. W. Lazio, "The Square Kilometre Array," Proc. IEEE, vol. 97, no. 8, pp. 1482–1496, Aug. 2009.
7. S. Jester and H. Falcke, "Science with a lunar low-frequency array: From the dark ages of the Universe to nearby exoplanets," New Astron. Rev., vol. 53, no. 1–2, pp. 1–26, May 2009.
8. R. T. Groves, "Analysis of the Radio Astronomy Explorer lunar orbit mission.," in AIAA & AAS, Astrodynamics Conference, 1972.
9. J. K. Alexander, M. L. Kaiser, J. C. Novaco, F. R. Grena, and R. R. Weber, "Scientific instrumentation of the Radio-Astronomy-Explorer-2 satellite," Astron. Astrophys., vol. 40, pp. 365–371, 1975.

10. J. K. Alexander and J. C. Novaco, “Survey of the galactic background radiation at 3.93 and 6.55 MHz,” Astron. J., vol. 79, p. 777, Jul. 1974.

11. D. Jones, R. Allen, J. Basart, T. Bastian, B. Dennison, K. Dwarakanath, W. Ericksong, D. Finley, M. Kaiser, N. Kassim, T. Kuiperl, R. Macdowall, M. Mahoney, R. Perley, R. Preston, M. Reiner, P. O. Rodriguez, R. Stone, S. Unwin, K. O. Weiler, G. Woan, and R. Wool, “The Astronomical Low Frequency Array : Explorer Mission for Radio Astronomy A Proposed Explorer Mission for Radio Astronomy,” in Radio Astronomy at Long Wavelengths, R. G. Stone, K. W. Weiler, M. L. Goldstein, and J.-L. Bougeret, Eds. American Geophysical Union, 2000, pp. 339–349.

12. R. J. MacDowall, S. D. Bale, L. Demaio, N. Gopalswamy, D. L. Jones, M. L. Kaiser, J. C. Kasper, M. J. Reiner, and K. W. Weiler, “Solar Imaging Radio Array (SIRA): A multi-spacecraft mission,” in Enabling Sensor and Platform Technologies for Spaceborne Remote Sensing, vol. 5659, no. May 2012, G. J. Komar, J. Wang, and T. Kimura, Eds. 2005, pp. 284–292.

13. J. O. Burns, J. Lazio, S. Bale, J. Bowman, R. Bradley, C. Carilli, S. Furlanetto, G. Harker, A. Loeb, and J. Pritchard, “Probing the first stars and black holes in the early Universe with the Dark Ages Radio Explorer (DARE),” Adv. Sp. Res., vol. 49, no. 3, pp. 433–450, Feb. 2012.

14. M. Bentum and A. J. Boonstra, “OLFAR - Orbiting Low Frequency Antenna for Radio Astronomy,” 20th Annu. Work. Circuits, Syst. Signal Process. ProRISC, pp. 1–6, 2009.

15. M. E. Knapp, “SOLARA/SARA: first steps toward a space-based radio interferometry constellation,” in 65th International Astronautical Congress (IAC), 2014.

16. D. Oberoi and J.-L. Pinçon, “A new design for a very low frequency space borne radio interferometer,” in American Geophysical Union Fall Meeting, 2003, no. 1988, p. 17.

17. K. T. Wong and M. D. Zoltowski, “Uni-Vector-Sensor ESPRIT for Multisource Azimuth, Elevation, and Polarization Estimation,” IEEE Trans. Antennas Propag., vol. 45, no. 10, pp. 1467–1474, 1997.

18. F. C. Robey, “High Frequency Geolocation and System Characterization (HFGeo) Phase 1B Proposers’ Day Briefing: HFGeo Phase 0 and Phase 1B Test and Evaluation,” 2012. [Online]. Available: http://www.iarpa.gov/images/files/programs/hfgeo/120710_Phase1B_Proposers_Day_Part2.pdf.

19. K. T. Wong and M. D. Zoltowski, “Closed-form direction finding and polarization estimation with arbitrarily spaced electromagnetic vector-sensors at unknown locations,” IEEE Trans. Antennas Propag., vol. 48, no. 5, pp. 671–681, 2000.

20. A. Nehorai and E. Paldi, “Vector-sensor array processing for electromagnetic source localization,” IEEE Trans. Signal Process., vol. 42, no. 2, pp. 376–398, 1994.

21. NIST, “Radio Station WWV,” 2015. [Online]. Available: http://www.nist.gov/pml/div688/grp40/wwv.cfm.

22. K. M. Górski, E Hivon,.A. J. Banday, B. D. Wandelt, F. K. Hansen, M. Reinecke, M. Bartelmann, “HEALPix: A Framework for High-Resolution Discretization and Fast Analysis of Data Distributed on the Sphere,” The Astrophysical Journal, Vol 622, No 2., 2005.

23. International Telecommunication Union, Radio noise P Series Radiowave propagation, vol. 11. 2013.

24. R. H. Dicke, “The Measurement of Thermal Radiation at Microwave Frequencies,” Rev. Sci. Instrum., vol. 17, no. 7, p. 268, 1946.

25. SPAWAR Systems Center PACIFIC, “Antenna Pattern Range.” [Online]. Available: http://www.public.navy.mil/spawar/pacific/cis/documents/antenna pattern range.pdf.

26. M. Knapp, F. Robey, R. Volz, F. Lind, A. Fenn, A. Morris, M. Silver, S. Klein, S. Seager, “Vector Antenna and Maximum Likelihood Imaging for Radio Astronomy”, Proc. IEEE 2016 Aerospace Conf., Mar. 2016.

27. A.J. Fenn and P.T. Hurst, Ultrawideband Phased Array Antenna Technology for Sensing and Communications Systems, The MIT Press, Cambridge, MA, 2015, pp. 255-267.

28. T.A. Milligan, Modern Antenna Design, 2nd Edition, IEEE Press, John Wiley, 2005, p. 260

29. Richard N. Grubb, Robert Livingston, Terence W. Bullett, “A new general purpose high performance HF Radar,” Proc. 2008 URSI General Assy Comm. G, [Online]. Available: http://www.ursi.org/proceedings/procGA08/papers/GHp4.pdf , [Accessed: 31-May-2016]

30. Ernest H. Nordholt and Frank Van Willigen. "A new approach to Active Antenna Design".IEEE Transactions on Antennas and Propagation, Vol AP-28, NO. 6, November 1980, pages 904 - 909.

31. Ronold King, “The rectangular loop antenna as a dipole,” IRE Transactions on Antennas and Propagation, Vol 7 , No. 1, Page(s): 53 - 61, Jan. 1959.

32. J.H. Meloling, J. W. Rockway, M. P. Daly, A. R. Monges, J. C. Allen, W. R. Nielsen, P. M McGinnis, R. B. Thompson, N. A. Mozaffar, “An Advanced HF Direction Finding Vector-Sensing Antenna System,” SPAWAR System Center Technical Report 2069, January 2015.

33. W. Li, R. Chen, N. Zhai, S. Li, R. Mittra, “Wideband Matching of an Electrically Small Antenna Using a Negative Impedance Converter Technique,” Proc of the 2012 IEEE Int. Sym. On Ant. and Prop., 2012.

34. Dylan Rudolph, Christopher Wilson, Jacob Stewart, Patrick Gauvin, Alan George, Herman Lam, Gary Crum, Mike Wirthlin, Alex Wilson, Aaron Stoddard, “CSP: A Multifaceted Hybrid Architecture for Space Computing,” Proc. 28th Annual AIAA/USU Conference on Small Satellites, 2014.

35. MARACOOS, “HF Radar Network”, 2016. [Online]. Available: http://marine.rutgers.edu/cool/maracoos/codar/radials/,

36. K. G. Budden, “Radio Waves in the Ionosphere,” Cambridge University Press, 2009.

37. S. T. Myers, “Polarization in Interferometry,” 12th Synthesis Imaging Workshop, June 2010. [Online] Available: http://www.aoc.nrao.edu/events/*synthesis/2010/lectures/MyersPolarization10.ppt.*

38. J. D. Kraus and R. J. Marhefka, “Antennas,” 3rd Edition, McGraw-Hill, p. 493, 2002.

39. Hewlett Packard Co., “HP 3562 Service Manual,” 1986.

BIOGRAPHY

Dr. Frank Robey *received BSEE (Summa Cum Laude) and MSEE degrees from U. Missouri-Columbia and D.Sc. EE in adaptive detection and beamforming from Washington University, St. Louis. He has been with MIT Lincoln Laboratory for 25 years. At Lincoln Laboratory he has been the lead for multiple fundamental and applied research initiatives including advanced sensor technology, coherent Multiple-Input Multiple-Output (MIMO) radar, electronic intelligence and next generation over-the-horizon radar. He spent two years on assignment as the Deputy Director of Smart Collection at IARPA/ODNI. He began his career as a precision instrument designer at Hewlett Packard and then at Emerson Electric.*

Mary Knapp *received a BS in Aerospace Engineering at MIT in 2011 and is currently a 4th year graduate student in MIT's Department of Earth, Atmospheric, and Planetary Science. She was awarded and NSF Graduate Research Fellowship in 2012. Her research focus is the detection and characterization of exoplanetary magnetic fields via low frequency radio emission. Her additional research interests include the development of small spacecraft for astronomy and planetary science She has participated in the development of the CubeSat ExoplanetSat (now renamed ASTERIA) since 2010. ExoplanetSat was developed at MIT for several years and is now in final development at JPL with an expected launch in late 2016/early 2017.*

Dr. Ryan Volz *received a BS degree in Aerospace Engineering from the Pennsylvania State University in 2007, an M.Phil degree in Engineering (Control Systems) from the University of Cambridge in 2008, and MS and PhD degrees in Aeronautics and Astronautics from Stanford University in 2009 and 2015, respectively. He was awarded an NDSEG graduate fellowship in 2008 and received third prize at the international URSI GASS 2011 student paper competition. He is currently a postdoctoral associate at the MIT Haystack Observatory researching radio measurement and signal processing methods that leverage sparsity.*

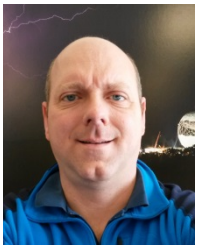

Dr. Frank D. Lind *studied at the University of Washington where he received a BS degree in Physics (with honors) and a BS degree in Computer Science in 1994. He then joined the UW Geophysics Program and pursued studies leading to the Doctor of Philosophy in Geophysics in 1999. His work there focused on Passive Radar Observations of the Aurora Borealis. He has worked at MIT Haystack Observatory for 15 years. His scientific and technical research focuses on radar and radio studies of the space environment, passive radar, incoherent scatter radar, ionospheric plasma physics, software radio and radar signal processing, and distributed sensor systems. At the Observatory he leads the technical team for the NSF sponsored Millstone Hill Geospace Facility and instrument development efforts for a variety of advanced radio telescopes, array radars, and distributed sensor networks. He is the former chair of USNC URSI Commission G.*

Dr. Alan J. Fenn *received a BS degree from the University of Illinois–Chicago and MS and PhD degrees from The Ohio State University, all in electrical engineering. He is a senior staff member in the RF Technology Group in the Advanced Technology Division at MIT Lincoln Laboratory. He is currently involved in the development of novel ultrawideband antennas and phased arrays for radar and communications applications. In 2000, Dr. Fenn was elected a Fellow of the IEEE for his contributions to the theory and practice of adaptive phased-array antennas. He is an author of more than 70 journal articles and conference papers in the field of antennas and adaptive phased array systems. He received the IEEE Antennas and Propagation Society's 1990 H.A. Wheeler Applications Prize Paper Award and the IEEE/URSI-sponsored 1994 International Symposium on Antennas JINA Award. He is currently serving as technical program chair for the 2016 IEEE International Symposium on Phased Array Systems and Technology.*

Kerry A. Johnson *received B.Eng. and M.Eng. degrees in electrical engineering from Stevens Institute of Technology. He currently holds the position of associate technical staff at MIT Lincoln Laboratory, focusing on novel sensors and small form factor electronics.*

Dr. Mark J. Silver *received a BS degree from the University of Wisconsin–Madison in engineering mechanics and MS and PhD degrees from the University of Colorado–Boulder in aerospace engineering. He is a staff member in the Mechanical Engineering Group in the Engineering Division at MIT Lincoln Laboratory. He has been with MIT Lincoln Laboratory for 5 years working in the area of design and analysis of terrestrial and spacecraft structures. His research areas include deployable spacecraft structures, precision alignment, composite materials and emerging computational analysis tools.*

Farshid Neylon-Azad *received a BS in Mechanical and Aerospace Engineering from Cornell University and an MS from Northeastern University in Mechanical Engineering. He is a staff member in the Advanced Capabilities and Technologies Group in the Space Systems and Technology Division at MIT Lincoln Laboratory. He has been at MIT Lincoln Laboratory for 5 years. At Lincoln Laboratory, Farshid's research areas have included; laser communications, EO/IR sensor development, satellite concept development and propulsion system design. Farshid began his career as an opto-mechanical engineer at L3 Integrated Optical Systems developing space-based optical instruments, where he spent 10 years prior to joining the laboratory.*

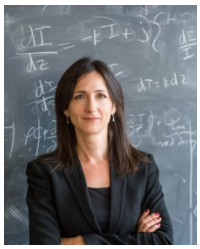

Professor Sara Seager *is an astrophysicist and planetary scientist at MIT. Her science research focuses on theory, computation, and data analysis of exoplanets. Her research has introduced many new ideas to the field of exoplanet characterization, including work that led to the first detection of an exoplanet atmosphere. Professor Seager also works in space instrumentation and space missions for exoplanets, including CubeSats, as a co-I on the MIT-led TESS, a NASA Explorer Mission to be launched in 2017, and chaired the NASA Science and Technology Definition Team for a "Probe-class" Starshade and telescope system for space-based direct imaging discovery and characterization of Earth analogs. Among other awards, Professor Seager is the 2012 recipient of the Raymond and Beverly Sackler Prize in the Physical Sciences, a 2013 MacArthur Fellow, and was elected to the National Academy of Sciences in 2015.*